Institute of Paper Science and Technology
Atlanta, Georgia

IPST TECHNICAL PAPER SERIES

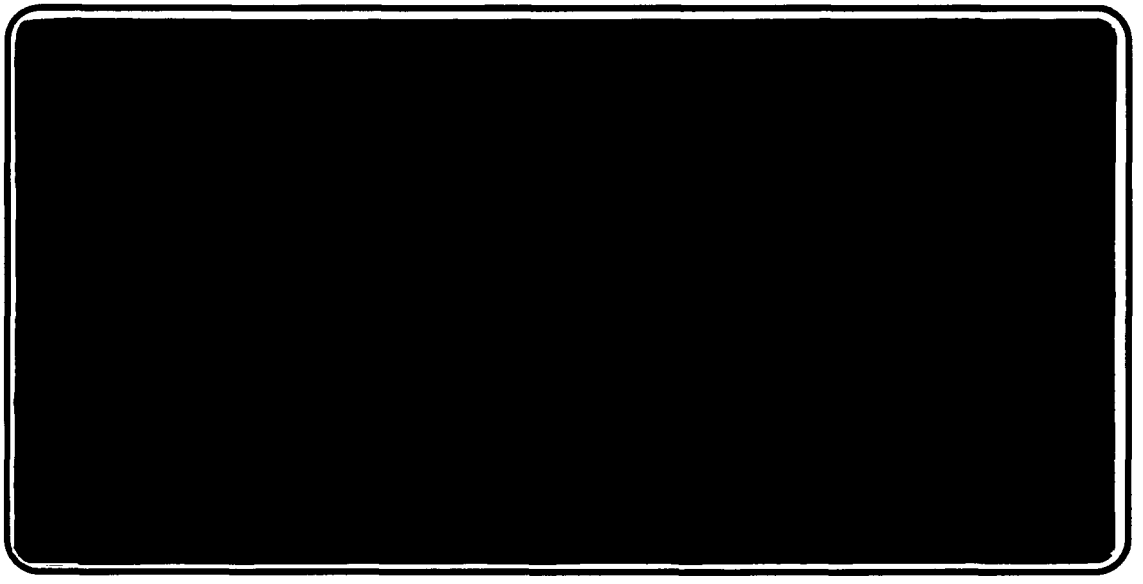

NUMBER 379

COMPUTATIONAL VISUALIZATION OF THREE-DIMENSIONAL FREE-SURFACE FLOWS

J.F. MC KIBBEN AND C.K. AIDUN

JUNE, 1991

Computational Visualization of Three-Dimensional Free-Surface Flows

J.F. McKibben and C.K. Aidun

Accepted for
1991 TAPPI Engineering Conference
Nashville, TN
September 1991

COMPUTATIONAL VISUALIZATION OF THREE-DIMENSIONAL FREE-SURFACE FLOWS

John F. McKibben
Graduate Student
Institute of Paper Science and Technology
Atlanta, Georgia

Cyrus K. Aidun
Assistant Professor
Institute of Paper Science and Technology
Atlanta, Georgia

ABSTRACT

We are developing a computational technique for analysis of three-dimensional free-surface flows. Although free-surface flows occur in a variety of processes within the pulp and paper industry (e.g., the forming section of the paper machine, coating processes, and finishing operations), the free-surface flows of primary interest to us are those that occur when black liquor is sprayed into a recovery furnace.

The computational technique being developed uses the Volume of Fluid (VOF) concept in conjunction with a third order accurate finite-difference solver for solution of the flow equations. The VOF method tracks the "fullness" of each computational cell in a finite-difference mesh as a function of time and thus is able to compute the free-surface location from this "fullness" function. At the end of each time step, the fluid is convected between the computational cells, yielding a new fluid configuration, and the process is repeated. Free-surface cells are defined as partially full cells with neighboring empty cells.

Of the many applications, we focus on simulation of three-dimensional flows of jets from circular nozzles and rectangular slots. The results of these simulations are presented as a combination of velocity vector plots, pressure contour plots, and, in free-surface problems, plots representing the fluid location. The added complexity of displaying the irregular shape of the free-surface is most effectively treated by animation of the free surface. Since our flows are transient, this animation represents the evolution of the surface with time but may also involve rotation or translation of a three-dimensional free surface in space.

NOMENCLATURE

$\mathbf{n}$	the unit vector normal to the free surface
$\mathbf{t}$	the unit vector tangent to the free surface
r,ϕ,z	cylindrical coordinate system
u,v,w	x, y, and z components of the velocity vector
x,y,z	Cartesian coordinate system
$\mathbf{g}$	acceleration due to gravity
$\mathbf{v}$	velocity vector

F fraction of a computational cell containing fluid
P pressure
R radius of curvature
γ surface tension
ν kinematic viscosity
ρ density
θ time
τ_{xx} $2\mu\left[\frac{\partial u}{\partial x}\right]$, the normal stress in the x-direction
τ_{xy} $\mu\left[\frac{\partial u}{\partial y}+\frac{\partial v}{\partial x}\right]$, the shear stress in the x-y plane
τ_{yy} $2\mu\left[\frac{\partial v}{\partial y}\right]$, the normal stress in the y-direction
Δ local difference in a variable

Subscripts
0 vapor phase
l left side of the computational domain
r right side of the computational domain
x x-direction component
y y-direction component

Superscripts
n current time step
n+1 next time step

INTRODUCTION

Free-surface fluid flow problems are often found in the pulp and paper industry. By free-surface flows we mean fluid flows where the liquid is at least partially bounded by a vapor phase, such as air, and where we can neglect variations in the velocity and pressure in the vapor phase.

Many of the processes in the pulp and paper industry involve free-surface flows, including headbox jets, the forming section, coating processes, finishing operations, and black liquor spraying, but our current work focuses solely on black liquor sprays, especially those from splash-plate type spray nozzles.

A splash-plate type spray nozzle (Figure 1) consists of a circular jet impinging upon a flat plate. Therefore, the initial portions of our work center on three-dimensional jet impingement. We will begin by describing the computational technique used to solve the flow equations to obtain velocity and pressure fields. Next, we will describe the additions to this procedure needed to track the free surface and impose the appropriate boundary conditions, and we will discuss the implications the presence of the free surface has upon the flow visualization. Finally, we will describe a three-dimensional jet impingement problem and the additional visualization requirements arising from three-dimensional flows.

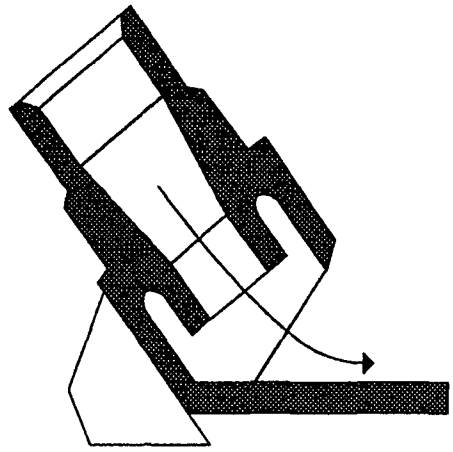

Figure 1. Schematic of a splash-plate black liquor nozzle.

COMPUTATIONAL TECHNIQUE FOR NAVIER-STOKES EQUATIONS

The computational fluid dynamics technique being developed uses the finite difference method to solve the equations representing the physical principles governing the motion of fluids. The equations, derived from conservation of mass and momentum, respectively, are

$$\nabla \cdot \mathbf{v} = 0 \qquad (1)$$

$$\underset{\text{inertial}}{\frac{\partial \mathbf{v}}{\partial \theta}} + \underset{\text{convective}}{\mathbf{v} \cdot \nabla \mathbf{v}} = \underset{\text{gravity}}{\mathbf{g}} - \underset{\text{pressure}}{\frac{1}{\rho} \nabla P} + \underset{\text{viscous}}{\nu \nabla^2 \mathbf{v}} \qquad (2)$$

These equations, first derived by Navier[1] and Stokes,[2] are known as the Navier-Stokes equations (NSE). Equation 1, commonly referred to as the continuity equation, requires that the amount of fluid in a computational cell remain constant (i.e., in - out = 0).

Equation 2 results from a momentum balance and is made up of inertial, convective, and gravitational forces and of a surface force consisting of pressure and viscous contributions. To interpret the relative importance of the convective and viscous contributions in the NSE, it is useful to define the dimensionless Reynolds number as the ratio of the convective and viscous forces. When the Reynolds number is low, the contribution of the viscous forces is dominant, and when the Reynolds number is high, the contribution of the convective forces dominates.

The SOLA Method

It is generally not possible to solve the NSE directly, so we must resort to numerical techniques. In our analysis, the pressure and velocity fields are computed using a SOLution Algorithm called SOLA originally formulated by Hirt et al.[3] They begin by specifying initial values for the velocities and pressure in the computational domain and applying the appropriate boundary conditions. A brief explanation of the SOLA method follows.

The NSE can be rewritten in terms of the velocity and pressure fields at the current and next times, n and n+1, respectively, by

$$\mathbf{v}^{n+1} = [\mathbf{v}^n + \Delta\theta(-\mathbf{v}^n \cdot \nabla\mathbf{v}^n + \mathbf{g} + \nu\,\nabla^2\mathbf{v}^n)] - \frac{\Delta\theta}{\rho}\nabla P^{n+1} \qquad (3)$$

Substituting Equation 3 into Equation 1 yields

$$\frac{\Delta\theta}{\rho}\nabla^2 P^{n+1} = \nabla \cdot [\mathbf{v}^n + \Delta\theta(-\mathbf{v}^n \cdot \nabla\mathbf{v}^n + \mathbf{g} + \nu\nabla^2\mathbf{v}^n)] \qquad (4)$$

Equation 4, a Poisson equation for pressure, can be solved for the pressure field at the next time by a number of numerical methods, such as successive over-relaxation. The resulting pressure field can then be substituted into Equation 3 to provide the new velocity fields. This procedure can be continued until any desired time has been reached.

Boundary Conditions

In order to complete a problem definition for confined flows, we must impose some combination of boundary conditions on the edges of our computational domain. Table 1 describes the mathematical formulation for four different boundary conditions on the left edge of the domain, defined as the y-z plane where x=0. The boundary conditions of the other five domain boundaries can be found by analogy.

Table 1. Example boundary conditions on the left wall for confined flows.

Boundary Condition	u	v	w	P
Frictionless Wall or Symmetry Plane	$u = 0$	$\frac{\partial v}{\partial x} = 0$	$\frac{\partial w}{\partial x} = 0$	$\frac{\partial P}{\partial x} = 0$
No-Slip Wall	$u = 0$	$v = 0$	$w = 0$	$\frac{\partial P}{\partial x} = 0$
Continuative Outlet	$\frac{\partial u}{\partial x} = 0$	$\frac{\partial v}{\partial x} = 0$	$\frac{\partial w}{\partial x} = 0$	$\frac{\partial P}{\partial x} = 0$
Periodic Condition	$u_l = u_r$	$v_l = v_r$	$w_l = w_r$	$P_l = P_r$

Finite Difference Approximations

The differential equations outlined above are solved by conversion to finite difference equations which are algebraic in nature. Equation 5 is an example of a simple finite difference formula.

$$\frac{\partial u}{\partial x} = \frac{\Delta u}{\Delta x} + \frac{\Delta x}{2!}\frac{\partial^2 u}{\partial x^2} + \frac{\Delta x^2}{3!}\frac{\partial^3 u}{\partial x^3} + \cdots + \frac{\Delta x^{m-1}}{m!}\frac{\partial^m u}{\partial x^m} + \cdots \qquad (5)$$

This equation, derived from a Taylor series, states that the partial derivative, $\partial u/\partial x$, can be replaced by a finite difference, $\Delta u/\Delta x$, plus additional terms containing Δx and higher derivatives of u. Since Δx is taken to be less than 1, these truncated terms are small and become even smaller as Δx decreases. In Equation 5, the series is truncated prior to the term containing Δx^1, so the finite difference formula is said to be first order accurate (the power of Δx in the largest term truncated in the series).

In our initial analysis, the viscous terms were treated using centered second order accurate finite differences, but the convective terms were computed using a linear combination of second order accurate centered finite differences and first order accurate upwind finite differences.[4,5] This combination takes advantage of the improved stability of upwind differences, while maintaining a portion of the accuracy of the centered differences.[6]

Our applications include black liquor sprays with Reynolds numbers greater than 1000 where the convective terms tend to dominate. Since, in our initial analysis, the dominant convective terms were less accurate than the viscous terms, the numerical accuracy of the entire analysis suffered.

To improve the accuracy of the convective terms, and thus the entire analysis, we implemented and tested three third order accurate finite difference schemes: QUICK (Quadratic Upstream Interpolation for Convective Kinematics),[7] a method developed by Kawamura and Kuwahara,[8] and a third order accurate upwind method initially derived by Agarwal.[9]

VALIDATION AND ACCURACY OF THE COMPUTATIONAL ANALYSIS

To test the effectiveness and accuracy of the third order accurate methods, we solved a lid-driven cavity problem (Figure 2). This problem consists of a box filled with fluid and having a moving lid. The lid-driven cavity is a common test problem for computational fluid dynamics codes and thus has been studied extensively. Below are comparisons of our results with those of Ghia et al.,[10] which have proved to be among the most precise solutions of this strongly nonlinear problem.

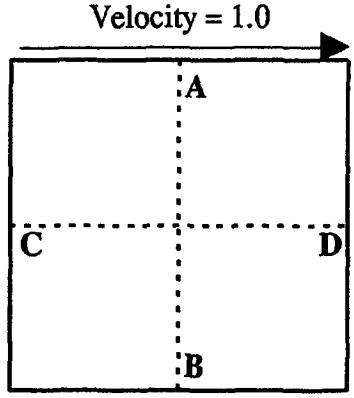

Figure 2. Schematic of the lid-driven cavity problem.

Ghia et al.[10] used a multigrid method with 128 computational cells in each direction, while our results were obtained using a finite difference method and only 40 cells in each direction. Figures 3 and 4 compare the results obtained by Ghia et al. with our four differencing schemes, SOLA, and the three third order accurate methods outlined above, for the convective terms in the NSE.

Two cases were run with each differencing scheme, the first with constant grid spacing and the second using a "graded" grid having smaller cells near the walls. Using smaller cells near the walls improves the accuracy of the entire simulation by better resolving the shear layers.

The results from Figures 3 and 4 are summarized in Table 2 and show that all of the third order accurate schemes yield much more accurate results than SOLA differencing. The third order accurate schemes give comparable results, and we were able to get within 5% of the results of Ghia et al. while using only 40 cells in each direction. Note that Kawamura and Kuwahara's method dropped from best to worst as the grid changes from constant to variable. This is because our derivation of the variable grid version of Kawamura and Kuwahara's method is inexact.

Table 2. % Error for lid-driven cavity cases.

Differencing Scheme	Constant	Variable
SOLA	54.3	38.8
Third order accurate upwind	13.0	4.2
QUICK	15.4	4.8
Kawamura and Kuwahara	12.4	6.7

FREE-SURFACE COMPUTATIONS

In free-surface problems there are the added complications of tracking the location of moving fluid boundaries and applying the appropriate conditions at these boundaries. The boundary conditions at the free surface arise from force balances normal and tangential to the interface between the two fluids.

Equations 6 and 7 are two-dimensional conditions for the tangential and normal force balances, respectively. Equation 6 states that the tangential stress vanishes at the free surface, and Equation 7 shows that the stress in the liquid normal to the interface is balanced by the pressure in the vapor phase and the surface tension force. Accurate knowledge of the location of the fluid boundary is extremely important for applying these conditions, especially for the computation of the surface curvature in the surface tension forces.[4,5]

$$\tau_{xx} n_x t_x + \tau_{xy}(n_x t_y + n_y t_x) + \tau_{yy} n_y t_y = 0 \qquad (6)$$

$$P - \tau_{xx} n_x^2 + 2\tau_{xy} n_x n_y + \tau_{yy} n_y^2 = P_0 - \gamma \left[\frac{1}{R}\right] \qquad (7)$$

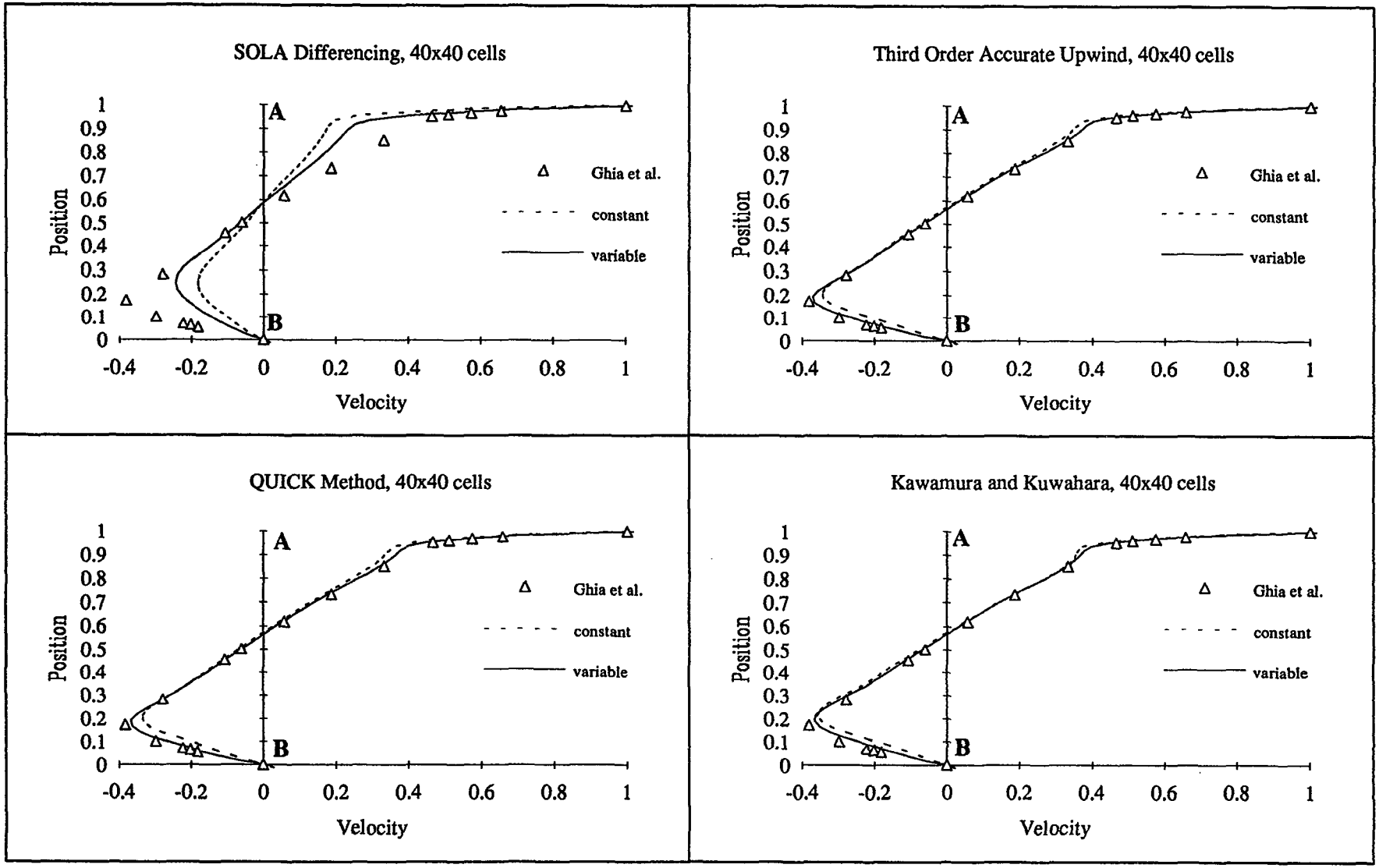

Figure 3. The U-component of velocity along the vertical centerline of the lid-driven cavity problem at Reynolds number 1000 for SOLA,[4,5] Agarwal,[9] QUICK,[7] and Kawamura and Kuwahara[8] differencing compared with the results of Ghia et al.[10]

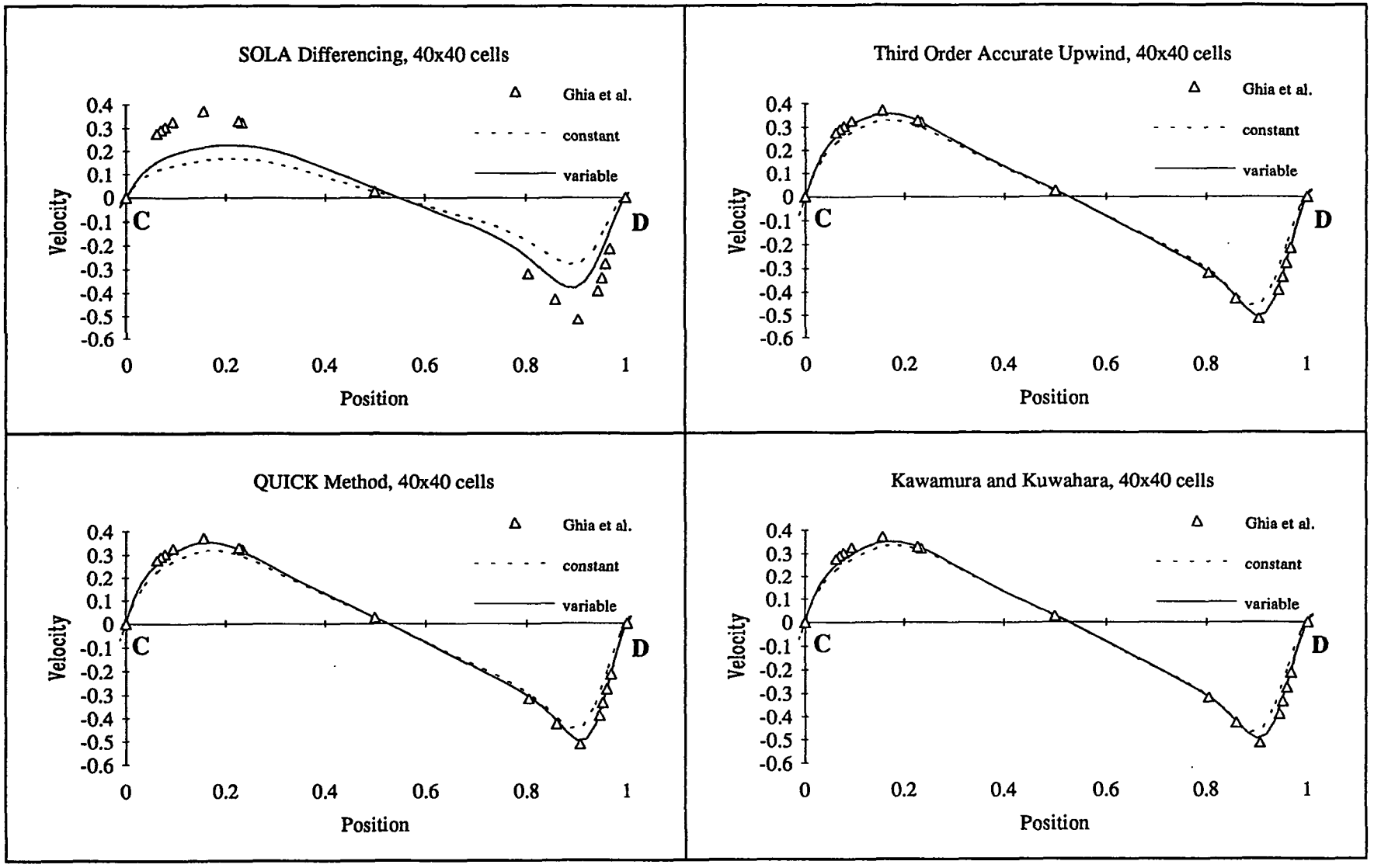

Figure 4. The V-component of velocity along the horizontal centerline of the lid-driven cavity problem at Reynolds number 1000 for SOLA,[4,5] Agarwal,[9] QUICK,[7] and Kawamura and Kuwahara[8] differencing compared with the results of Ghia et al.[10]

The VOF Method

In the VOF method the location of the fluid boundary must be determined from the "fullness" function, a step function describing the presence of fluid at each point within the computational domain.[11] This function is averaged over each computational cell to give F, the fraction of each cell containing fluid. The surface location and shape are calculated from the F values in the computational cells surrounding the free-surface cells, and the free-surface boundary conditions are applied.

The addition of the F function requires an additional differential equation describing the variation of F as a function of space and time. This convection equation for F is

$$\frac{\partial F}{\partial \theta} + \mathbf{v} \cdot \nabla F = 0 \qquad (8)$$

Equation 8 is solved explicitly at the end of each time step, following Equation 3 above, to yield the new fluid configuration:[4,5]

$$F^{n+1} = - \Delta\theta \, (\mathbf{v}^{n+1} \cdot \nabla F^{n}) \qquad (9)$$

Free-Surface Display

The presence of free surfaces complicates the display of the computational results. Normally, computational flow visualization consists of a combination of velocity vector plots and pressure contour plots. With free surfaces present, we need some method of displaying the fluid boundaries. In two-dimensional problems this is most easily accomplished by drawing filled regions where the fluid is present.

TWO-DIMENSIONAL FREE-SURFACE EXAMPLE

To verify the accuracy of our code for free-surface problems and to test two-dimensional free-surface display methods we began by studying the die-swell problem. The term die-swell is used to describe the expansion of a fluid as it is extruded from a die at low Reynolds number. As the Reynolds number increases, the swelling decreases, and ultimately the fluid shrinks.

In our tests we studied extrusion from a two-dimensional Cartesian slot at Reynolds number 300 (Figure 5). We used results from the commercial code FIDAP[12] and from Omedei[13] for comparison. FIDAP and Omedei solved the Reynolds number 300 die-swell problem in the absence of gravity and surface tension and predicted swells of -15.24% and -15.52%, respectively.

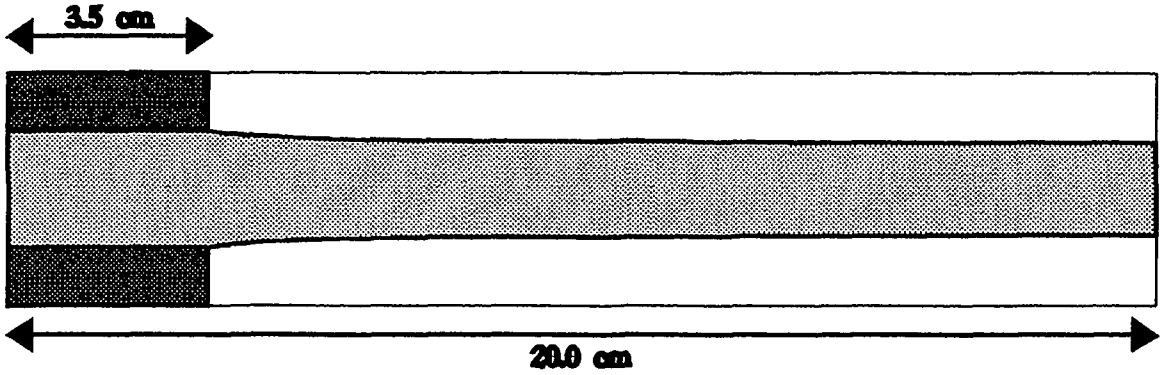

Figure 5. Schematic of a Cartesian die-swell problem.

For the die-swell problem at Reynolds number 300, we found a variety of die swells that depend both on the number of cells in each direction and, most important, on the minimum cell spacings adjacent to the corner of the die. The results from five cases using QUICK differencing are presented in Table 3. Case 4 with 40 cells in the width of the jet and 300 cells in the length of the jet yielded -15.28 %, which compares favorably with -15.24 % and -15.52 % reported by FIDAP[12] and Omedei,[13] respectively.

Using a domain length of 25 cm in case 5 rather than 20 cm in case 3 test the assumption that the flow is fully developed at the outlet. Comparing these cases indicates that the 20 % increase in domain length produced only a 0.2 % change in thickness which supports this assumption.

Table 3. Sample swell ratios from die-swell problem at RE=300.

CASE	X cells	Y cells	Min ΔX	Min ΔY	%Swell
1	30	160	0.03333	0.03333	-14.23
2	30	200	0.02	0.02	-15.15
3	30	200	0.015	0.015	-15.24
4	40	300	0.01	0.01	-15.28
5*	30	300	0.02	0.02	-15.30

* Case 5 had a domain length of 25 cm rather than 20 cm.

Some sample results of filled fluid plots from case 4 are presented in Figure 6. The average inlet velocity for this case was 1 cm/s, and the sample plots are times 0.0, 5.0, 10.0, 15.0, 20.0, and 25.0 seconds, respectively.

THREE-DIMENSIONAL FREE-SURFACE FLOW VISUALIZATION

Displaying these data becomes more difficult when flows are three-dimensional. For instance, velocity data displayed as vector fields in three dimensions would be unintelligible.

Commonly, three-dimensional data are displayed as a series of two-dimensional slices which the viewer must attempt to visually reconstruct into a three-dimensional image. These two-dimensional slices can be very useful in displaying flows that change by only a small amount

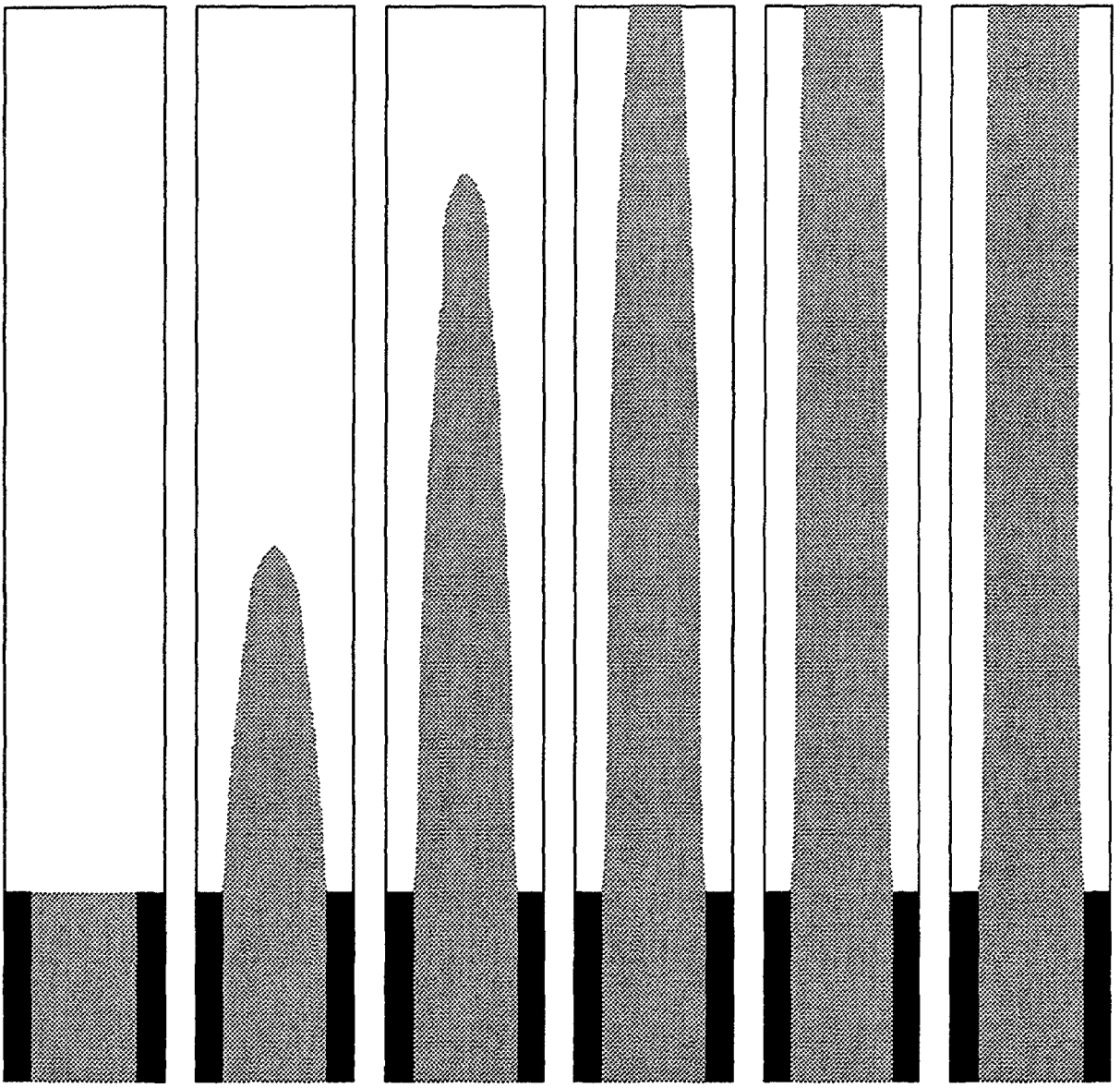

Figure 6. Views of a Cartesian die-swell problem at RE 300 in the absence of surface tension and gravity at 0, 5, 10, 15, 20, and 25 seconds.

along one direction (i.e., r-z slices of constant ϕ from a cylindrical flow that is nearly axisymmetric).

In our analysis we use two-dimensional slices to show velocity information with filled fluid location, but we use three-dimensional isosurface plots for the free-surface location. These isosurfaces are the three-dimensional analogue of the two-dimensional F contours.

Currently, our three-dimensional isosurfaces are drawn using wire frames. This means that the surface is made up of a series of line segments. Since the nodes of the wire frame are constantly spaced in two dimensions, we have visual cues to help see the three-dimensional variations.

We have begun studying the use of solid surface patches with a light model to better show the three-dimensional detail. This process involves the use of a "light" located in the three-dimensional space with the viewer's "eye" also oriented in the three-dimensional space. The surface can be computationally "illuminated" by computing the amount of light reflected from the surface to the eye and adjusting the brightness of the surface accordingly. The amount of light reflected can be altered by defining the reflective properties of the surface and adding light sources. In addition, we can study detailed features of the surface by moving the light position and/or the eye position and orientation relative to the three-dimensional isosurface.

Three-Dimensional Sample Problem

We are using a jet impingement problem as a three-dimensional example (Figure 7). This problem consists of a section of an infinite slot jet of Reynolds number 500 impinging upon an infinite flat plate at a 15-degree angle. The jet is water from a 0.5 cm nozzle with an average initial velocity of 251 cm/s. The dimensions of the computational domain are 15x2x1 cm in x, y, and z directions, respectively, with the governing equations discretized using 90x40x10 cells in the domain.

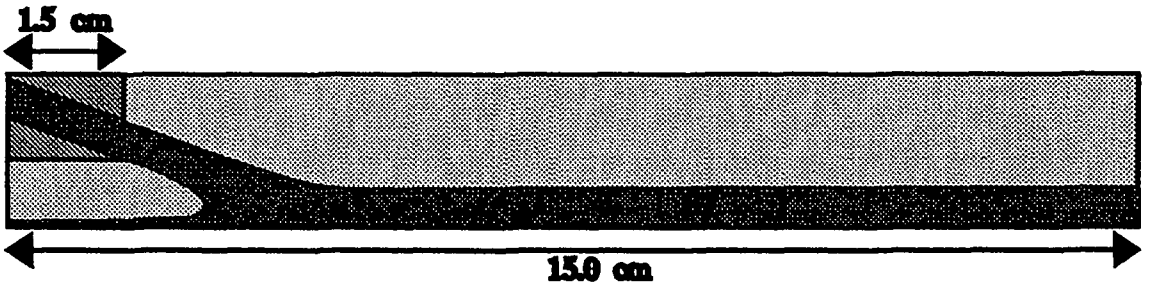

Figure 7. Two-dimensional cross section of the three-dimensional jet impingement problem.

Figure 8 contains sample wire frame plots from the 15-degree slot jet impingement problem at times 0.0, 0.02, 0.04, 0.06, 0.08, and 0.1 seconds. These plots, with additional intermediate figures, can be combined to produce animated videos of the free-surface movement. The portion of the fluid flowing backward has been omitted from the three-dimensional plots for clarity.

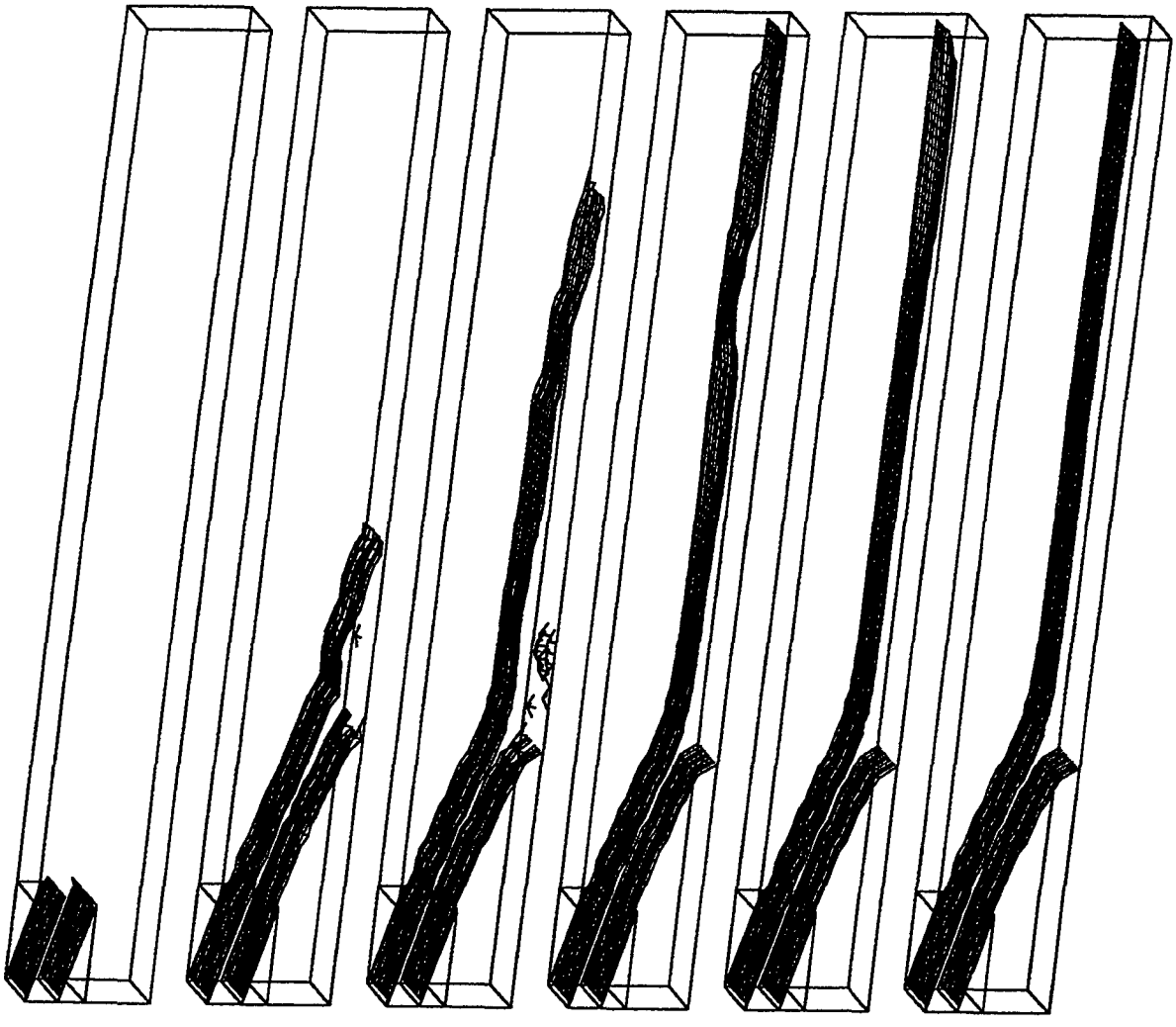

Figure 8. Views of the top and bottom surfaces from a section of an infinite slot jet at RE 500 impinging on a frictionless wall at 0.0, 0.02, 0.04, 0.06, 0.08, and 0.1 seconds.

SUMMARY

We have developed a computational analysis for three-dimensional free-surface flows and have shown this analysis to be accurate both for confined flows and two-dimensional free-surface flows. In addition, we presented three-dimensional flow results that give examples of the visualization possibilities for animated transient free-surface movement. This analysis forms the basis for our continued work toward simulation of the splash-plate type black liquor nozzle.

REFERENCES

1. M. Navier, Mem. de l'Acad. des Sciences, 6:389(1822).

2. G. G. Stokes, Trans. Cambridge Phil. Soc., 8:287(1845).

3. C. W. Hirt, B. D. Nichols, and N. C. Romero, SOLA - A Numerical Solution Algorithm for Transient Fluid Flows, Los Alamos Report LA-5852, 1975.

4. M. D. Torrey, L. D. Cloutman, R. C. Mjolsness, and C. W. Hirt, NASA-VOF2D: A Computer Program for Incompressible Flows with Free Surfaces, Los Alamos Report LA-10612-MS, Dec. 1985.

5. M. D. Torrey, R. C. Mjolsness, and Stein, L. R.; NASA-VOF3D: A Three-Dimensional Computer Program for Incompressible Flows with Free Surfaces, Los Alamos Report LA-11009-MS, July 1987.

6. P. J. Roache, Computational Fluid Dynamics, Hermosa Publishers, Albuquerque, NM, 1976.

7. B. P. Leonard, Computer Methods in Applied Mechanics and Engineering, "A Stable and Accurate Convective Modeling Procedure based on Quadratic Upstream Interpolation," 19:59-98(1979).

8. T. Kawamura and K. Kuwahara, "Computation of High Reynolds Number Flows Around a Circular Cylinder with Surface Roughness," AIAA Paper AIAA-84-0340, Jan. 1984.

9. R. K. Agarwal, "A Third-Order-Accurate Upwind Scheme for Navier-Stokes Solutions at High Reynolds Numbers," AIAA Paper AIAA-81-0112, 1981.

10. U. Ghia, K. N. Ghia, and C. T. Shin, Journal of Computational Physics, "High-Re Solutions for Incompressible Flow Using the Navier-Stokes Equations and a Multigrid Method," 48:387-411(1982).

11. C. W. Hirt and B. D. Nichols, Journal of Computational Physics, "Volume of Fluid (VOF) Method for the Dynamics of Free Boundaries," 39:201-225(1981).

12. FIDAP User's Manual, Fluid Dynamics International Inc., Evanston, IL, 1990, Revision 5.0, 1st Edition, p. 6-1.

13. J. Omedei, Computers and Fluids, "Computer Solutions of a Plane Newtonian Jet with Surface Tension," 7, (1979).

ACKNOWLEDGMENTS

Portions of this work were used by J. F. M. as partial fulfillment of the requirements for the Ph.D. degree at the Institute of Paper Science and Technology.

This research was conducted using the Cornell National Supercomputer Facility, a resource of the Center for Theory and Simulation in Science and Engineering at Cornell University, which is funded in part by the National Science Foundation, New York State, and the IBM Corporation.